Chapter 13
On the Derivation and Application of a Finite Strain Thermo-viscoelastic Material Model for Rubber Components

Jonas Schröder, Alexander Lion, and Michael Johlitz

Abstract This contribution deals with a modified material model of the finite thermoviscoelasticity for the efficient calculation of the dissipative self-heating of elastomer components. The occurrence of critical temperatures, which can lead to loss of functionality or component failure, can be identified at an early stage. Here, the focus lies on industrial applicability, which, in addition to calculation time and quality, also includes the experimental effort required to identify the material parameters. This contribution starts with the formulation of a thermomechanically consistent constitutive model. For this purpose, an appropriate description of the kinematics and the derivation of the constitutive relationships is carried out. These are transferred in a suitable way into the form used by the commercial finite element software ABAQUS and implemented as a thermomechanically fully coupled problem. Furthermore, an industrially applied elastomer material is characterised and the model is parameterized in a special method by selecting the potential function. Finally, the validation of the model and its parameterization are carried out by means of experimental component tests.

Keywords: Finite element implementation · Fully coupled · Finite thermoviscoelasticity · Dissipative heating · Thermomechanics · Elastomer

13.1 Introduction

Due to their typical material characteristics, elastomer components are used in almost all areas of engineering and across industries (Elsner et al, 2012). In addition

Jonas Schröder · Alexander Lion · Michael Johlitz
Institute of Mechanics, Faculty for Aerospace Engineering, Bundeswehr University Munich, Germany,
e-mail: jonas.schroeder@unibw.de, alexander.lion@unibw.de, michael.johlitz@unibw.de

H. Altenbach and A. Öchsner (eds.), *State of the Art and Future Trends in Material Modeling*, Advanced Structured Materials 100,
https://doi.org/10.1007/978-3-030-30355-6_13

to the chemical properties, the physical behaviour of the material is of primary importance in the selection process. These include the reversible absorption of large deformations at comparatively low loads as well as the vibration and noise decoupling properties (Koltzenburg et al, 2013). In many cases, these components are subject to large cyclic deformations which result in dissipation-induced self-heating. Depending on the application, elastomer components may also be exposed to elevated ambient temperatures. Increased component temperatures can lead to impermissible changes in the material properties, i.e. to loss a function or total failure. Therefore, it is important to identify critical temperatures and loads early in the development process. The aim is to replace cost-intensive prototype tests with FEM[1] simulations. The concept shown in Fig. 13.1 is used for the simulation of component temperatures. The input parameters of this concept are primarily the component geometry and the material properties. By the suitable formulation of the material model, the relevant material behaviour is taken into account and used for the calculation. The parameterization of the model is carried out by experimental material characterization. Subsequently, boundary conditions and material properties are assigned to the discretized component geometry such that the local temperature and the load curves can be calculated.

The second section focuses on the phenomenological analysis of elastomer materials: First the typical material behaviour is explained based on the material structure, then a selection of the modelled relevant phenomena is made by assessing their responsibility for self-heating. The following section contains the continuum mechanical material modelling. A suitable description of the kinematics is introduced by multiplicative decomposition of the deformation gradient in order to represent different types of deformation. In addition, the constitutive relationships are derived by evaluation of the Clausius-Duhem inequality for a general potential function. The

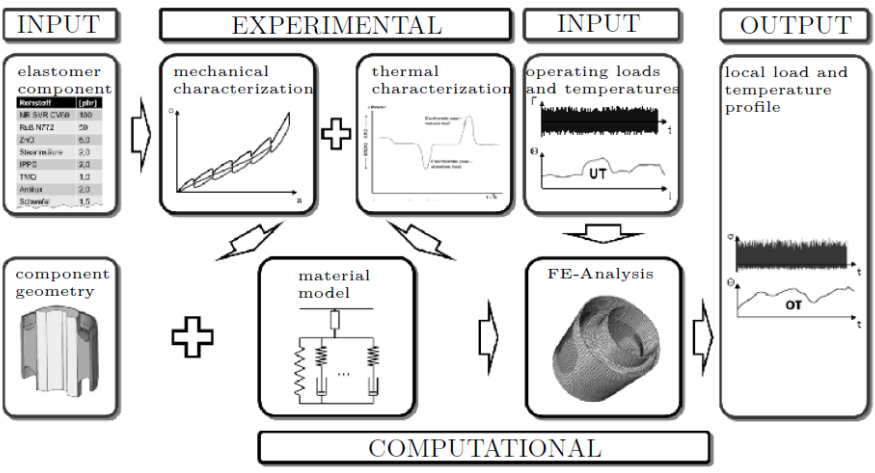

Fig. 13.1 Concept for the derivation of the dissipative heating of elastomer components

[1] FEM is the abbreviation of finite element method

ABAQUS-related heat conduction equation is also specified. The fourth section deals with the FE implementation. From the heat conduction equation in combination with the balance of momentum, a fully coupled functional is obtained by applying Galerkin's method. This is linearised for the iterative calculation with the Newton method. Next, the required constitutive relationships and their associated consistent tangent operators are derived. The selection of the potential functions and the resulting evaluations of the state vectors and tangent operators are similary carried out in the fifth section, as well as the conversion into the formulation required for the UMAT[2] implementation. In section six, the validation of the material model and its parametrization is carried out. This begins with the development of the computational model and concludes with the comparison of simulated and experimentally determined characteristics. Chapter seven concludes with a discussion and evaluation of the model quality and efficiency with regard to industrial applicability. In addition, an outlook on future trends and prospects is given.

13.2 Elastomer Structure and Behaviour

This section provides the basic considerations leading to the selection of a suitable material model. For this purpose, the typical behaviour of elastomer materials is first explained on the basis of the chemical structure and then assessed with regard to the influence on the dissipative self-heating process. Elastomers are weakly crosslinked polymers which exhibit the characteristic entropy-elastic behaviour at operating temperatures. The meaning of this term is deduced from the macroscopic view of the material. Detailed descriptions of the molecular structure can be found in the standard literature, e.g. Treloar (1975); Tobolsky et al (1971) or Schwarzl (2013). The chain molecules perform thermally disordered movements and have a large number of moving segments. Thus, they occupy the thermodynamically and statistically most probable arrangement, namely the one of maximum entropy. Therefore, the molecules are strongly entangled in the material. The elasticity can be traced back to the mobility of the molecules above the glass transition, which is limited by cross-links and entanglements. Polymer chains are initially entangled. Under external stress they rearrange themselves such that the chains get stretched and thereby change the state of order. Due to that, the directed chains exhibit less entropy and have the tendency to take up a state of higher disorder or entropy. Therefore, rubber elasticity is also called entropy-induced (Tobolsky, 1967; Treloar, 1975). This enables large reversible deformations with almost incompressible material behaviour, whereby the stress depends non-linearly on the strain (Rivlin and Saunders, 1951), but approximately linearly on the temperature (Anthony et al, 1942). However, under sufficiently small constant deformations, a drop in the engineering stress with increasing temperature can be observed. This phenomenon is generally known as the thermo-elastic inversion and is based on the overlay of thermal expansion and entropy elasticity. The deformation

[2] User-defined material model (UMAT) in ABAQUS can be used to define the mechanical constitutive behaviour of a material.

during an adiabatic process results in a temperature change, also known as Joule-Gough effect (Gough, 1805; Joule, 1859). The reason for this is the compensation of the deformation-related decrease in entropy due to an increase in temperature. Since, time-dependent internal sliding and rearrangement processes of molecules also occur, elastomers are also referred as viscoelastic materials. Infinitely slow deformation processes, denoted as quasi-static, lead to thermodynamic equilibrium states. On this occasion the viscous components play a minor role. In the case of cyclic dynamic loading, a load history and strain rate dependent hysteresis loop occurs. The enclosed area is a measure of the mechanical energy converted into thermal energy and is defined as dissipation. The temperature influence on the viscoelastic material properties, which can be also observed, is based on the fact that sliding and rearrangement processes accelerate with increasing temperature. The relationship between temperature and rate dependence can be described with the time-temperature superposition principle. In order to adapt the material properties to the technical application, fillers in addition to chemical additives are added to improve the mechanical properties. Due to the different types of interaction, the defined properties must be adjusted with regard to a common optimum. Filled elastomers show significant differences in their characteristic behaviour compared to unfilled elastomers. With filled materials, the complex temperature behaviour of the interactions between the fillers and the elastomer matrix superimposes to the entropy elasticity, such that a completely different stiffness characteristic can be observed. The elastomer/filler interaction leads to a characteristic softening within the first loading cycles. The so-called Mullins-effect (Mullins, 1948) results from the breaking and rearrangement of weak polymer chains and the successive breakage of certain sections of the filler network until a more or less "constant" material behaviour is achieved. The viscoelastic behaviour shows a non-linear dependence on the loading. This amplitude dependence is also known as the Payne-effect (Payne, 1962).

In summary, it can be stated that elastomers, due to their molecular structure, can take up elongations of several 100%, show no major volume change and return to their original shape completely when the load is removed. In addition, elastomers exhibit a marked viscoelastic behaviour, such that cyclic mechanical loads at adequate amplitudes and frequencies are leading to significant energy dissipation. Therefore, elastomer components can heat up strongly under insufficient heat removal. The temperature change leads to a change in the viscoelastic material properties and generates thermal strains or thermally induced stresses. In the case of filled elastomers, thermo-elastic effects play only a minor role in self-heating due to the dependencies described above.

13.3 Continuum Mechanical Material Modelling

Material theory is a subsection of continuum mechanics which deals with material models. It provides general principles and systematic methods for the formulation of mathematically and thermodynamically consistent models to describe the individual

properties of a material body. The derivation of constitutive relations follows the principles of rational thermomechanics. Here, the second law of thermodynamics acts as a restriction to obtain a thermomechanically consistent constitutive equation. In order to formulate consistent models, the dissipation postulate must be fulfilled. In addition, the axiomatic principles of material theory must be followed. Multiplicative decomposition of the deformation gradient allow to consider different deformation mechanisms. The free energy density is an appropriate thermodynamic potential to model the material properties, whereby its independent variables, or arguments must be defined. At the beginning of this section, the basics and contexts, which are necessary for understanding the following considerations, are explained. This includes the balance relations of thermomechanics and the resulting principle of irreversibility. In addition, a proper description of the kinematics is introduced, the independent variables are defined and the constitutive relationships are derived from the potential.

13.3.1 Balance Equations

This section presents the classical balance equations of thermomechanics. They are independent of the special properties of the continuum, since they describe universally valid laws of nature. They can be formulated globally for the entire material body in integral form, or locally in differential form. Furthermore, the balance equations can be formulated for each configuration. In the following, the equations are described in local form using variables related to the reference configuration.

13.3.1.1 Conservation of Mass

$$\frac{\partial}{\partial t}\rho_0(\mathbf{X},t) = 0 \qquad \Rightarrow \qquad \rho_0 = \rho_0(\mathbf{X}) = \text{constant} \tag{13.1}$$

ρ_0 is the density related to the reference configuration. It does not depend on time, thus it depends only on the vector of the material points in the reference configuration $\mathbf{X}$.

13.3.1.2 Balance of Linear Momentum

$$\rho_0\dot{\mathbf{V}}(\mathbf{X},t) = \text{Div}\,(\mathbf{P}) + \rho_0\mathbf{b} \tag{13.2}$$

The time derivative of the momentum on the left hand side is expressed by the time derivative of the material velocity field $\dot{\mathbf{V}}$ which is weighted with the density. On the right hand side the force density, composed of the divergence in relation to the

material coordinates of the first Piola-Kirchhoff stress tensor $\mathbf{P}$ and body force per unit volume $\rho_0\mathbf{b}$.

13.3.1.3 Balance of the Angular Momentum

$$\mathbf{S} = \mathbf{S}^{\mathrm{T}} \qquad \text{or} \qquad \mathbf{P} \cdot \mathbf{F}^{\mathrm{T}} = \mathbf{F} \cdot \mathbf{P}^{\mathrm{T}} \tag{13.3}$$

The quantity $\mathbf{S}$ is the second Piola-Kirchhoff stress tensor. Its symmetry follows from the local form of the balance of rotational momentum. The first Piola-Kirchhoff stress tensor $\mathbf{P}$ is generally not symmetric and the characteristic described above holds, where $\mathbf{F} = \mathrm{Grad}\left(\mathbf{x}\right)$ is the deformation gradient. Here $\mathrm{Grad}(\circ)$ is the gradient operator with respect to the material coordinates. The vector $\mathbf{x}$ is the current position of the material point $\mathbf{X}$ at time t in the current configuration.

13.3.1.4 Balance of Energy

$$\rho_0 \dot{e} = \mathbf{S} : \dot{\mathbf{E}} - \mathrm{Div}\left(\mathbf{q}_0\right) + \rho_0 r \tag{13.4}$$

The energy balance provides the temporal change of the specific internal energy $\rho_0\dot{e}$. It consists of the volume-related stress power $\mathbf{S} : \dot{\mathbf{E}}$ where $\dot{\mathbf{E}}$ is the time derivative of the Green-Lagrange strain tensor and the heat exchange. The vector $\mathbf{q}_0$ denotes the Piola-Kirchhoff heat flux vector and $\rho_0 r$ is the heat source per unit volume. This equation is also known as the first law of thermodynamics.

13.3.1.5 Balance of Entropy

$$\rho_0 \dot{\eta} + \mathrm{Div}\left(\frac{\mathbf{q}_0}{\theta}\right) - \rho_0 \frac{r}{\theta} = \rho_0 \tilde{\eta} \geq 0 \tag{13.5a}$$

$$\Leftrightarrow \tilde{\eta} \geq 0 \tag{13.5b}$$

On the left hand side, the temporal change in the entropy per unit volume is described by the expression $\rho_0\dot{\eta}$. The heat supply per unit time related to the thermodynamic temperature θ is used to calculate the entropy supply. Here, $\frac{\mathbf{q}_0}{\theta}$ is the entropy flux and $\frac{r}{\theta}$ is the specific entropy source, whereby θ denotes a time-dependent scalar field. On the right hand side the specific entropy production $\tilde{\eta}$ is opposed. For all thermomechanical admissible processes, the entropy production $\tilde{\eta}$ must be greater than or equal to zero. The balance is also known as the second law of thermodynamics.

13.3.1.6 Dissipation Inequality

As mentioned above, the constitutive relations are derived from the Helmholtz free energy density as a function of deformation and temperature. The equations presented previously are valid for all material models of continuum mechanics, such that the

Legendre transform of thermodynamic potentials is used to transform the specific internal energy $\rho_0 e$ into the Helmholtz free energy per unit mass:

$$\Psi = e - \theta\eta \tag{13.6}$$

The insertion of the time derivative of the free energy function (13.6) into the entropy inequality (13.5a) leads to the well known Clausius-Duhem inequality:

$$\rho_0 \dot{\Psi} + \mathbf{S} : \dot{\mathbf{E}} - \rho_0 \dot{\theta}\eta - \frac{\mathbf{q}_0}{\theta} \operatorname{Grad} \theta \geq 0 \tag{13.7}$$

Here Grad$(\circ)$ is the gradient operator with respect to the material coordinates. The entire model must satisfy this inequality, which represents the second law of thermodynamics, to obtain a thermomechanically consistent material model.

13.3.2 Quasi-incompressible Modified Thermoviscoelasticity

Subsequently, this contribution emphasises thermomechanically consistent material modelling. For this purpose, the concept of the model is motivated on the basis of a rheological representation. Based on these findings, the description of suitable kinematics and the definition of independent variables is carried out. Finally, the constitutive relations are derived respecting thermomechanical consistency. The development of thermomechanical material models has been the focus of the following research activities Lion (2000); Johlitz (2015); Dippel et al (2014); Reese (2001). It should be mentioned that this list is not complete. The implementation of thermomechanically coupled material models has been the subject of Miehe (1988); Simo and Miehe (1992); Anand (1985); Arruda et al (1995); Heimes (2004); Bröcker and Matzenmiller (2008); Anand et al (2009); Naumann and Ihlemann (2011); Bröcker (2013); Hamkar (2013) or Lejeunes et al (2018). The solution of thermomechanical coupled processes has been investigated among by Glaser (1992) or Erbts and DüSter (2012). Based on the model of classical viscoelasticity, the deduced material model can be motivated. The usage of rheological elements as a method of representation has not only the advantage of special illustration, it also leads to thermomechanically consistent models. Moreover, these elements can be extended easily to three-dimensional states of stress and strain and nonlinearities. In consequence, the model presented in Fig. 13.2 is introduced. The part of the free energy that depends only on the temperature is described by Ψ_{th}. The total energy stored in the springs can be additively allocated to the respective springs. The equilibrium part of the free energy Ψ_{eq} is assigned to the single spring. In addition to the elastic behaviour, it represents the equilibrium part of the stress $\mathbf{P}_{eq}$. The springs of the Maxwell elements represent the overstresses $\mathbf{P}^{(k)}_{neq}$ and can be linear or non linear. The free energies $\Psi^{(k)}_{neq}$ are related to them. The temperature-dependent viscosities $\check{\eta}^{(k)}(\theta)$ describe the rate dependence of the damper elements. The structure

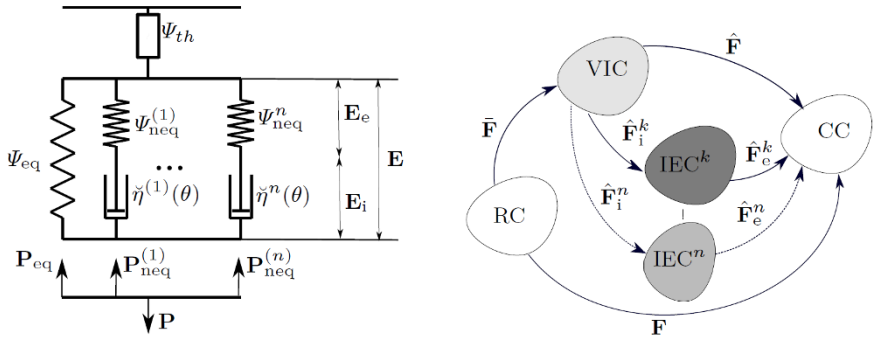

Fig. 13.2 Rheological representation of modified finite thermoviscoelasticity (left), decomposition of the deformation gradient (right): The reference configuration (RC), volumetric-isochoric intermediate configuration (VIC), elastic-inelastic intermediate configurations (EIC) and the current configuration (CC)

of the model mapping of the dissipation implies a separation of elastic and inelastic deformations.

13.3.2.1 Kinematics

First of all, large deformation require a distinction between the reference and the current configuration. In order to distinguish different types of deformation, it is necessary to split the deformation gradient multiplicatively. Some intermediate configurations will be introduced on this occasion. The first multiplicative decomposition of the deformation gradient is carried out to split the local deformation into volumetric and isochoric parts and simplifies the representation of quasi incompressible behaviour. For this purpose the volumetric-isochoric intermediate configuration (Flory, 1961) is introduced

$$\mathbf{F} = \hat{\mathbf{F}} \cdot \bar{\mathbf{F}} \qquad \text{with} \qquad \hat{\mathbf{F}} = J^{-\frac{1}{3}}\mathbf{F} \qquad \text{and} \qquad \bar{\mathbf{F}} = J^{\frac{1}{3}}\mathbf{I} \tag{13.8}$$

with the definition of the volumetric part $\bar{\mathbf{F}}$ of the deformation and the isochoric part $\hat{\mathbf{F}}$ using the determinant $\det(\mathbf{F}) = J$. Finally, the isochoric part is divided multiplicatively into purely elastic components $\hat{\mathbf{F}}^{(k)}_{\mathrm{e}}$ and inelastic components $\hat{\mathbf{F}}^{(k)}_{\mathrm{i}}$. This multiplicative split introduces elastic-inelastic intermediate configurations (Lubliner, 1985):

$$\hat{\mathbf{F}} = \hat{\mathbf{F}}^{(k)}_{\mathrm{e}} \cdot \hat{\mathbf{F}}^{(k)}_{\mathrm{i}}, \tag{13.9}$$

where the index $[\circ]^{(k)}$ indicates the respective Maxwell element. At this point, the right elastic Cauchy-Green deformations tensor $\hat{\mathbf{C}}^{j}_{e}$ and the right inelastic Cauchy-Green deformations tensor $\hat{\mathbf{C}}^{j}_{i}$ are defined:

$$\hat{\mathbf{C}}_e^{(k)} = \hat{\mathbf{F}}_{\mathrm{e}}^{\mathrm{T}(k)} \cdot \hat{\mathbf{F}}_{\mathrm{e}}^{(k)} \tag{13.10}$$

$$\hat{\mathbf{C}}_i^{(k)} = \hat{\mathbf{F}}_{\mathrm{i}}^{\mathrm{T}(k)} \cdot \hat{\mathbf{F}}_{\mathrm{i}}^{(k)} \tag{13.11}$$

The tensor $\hat{\mathbf{L}}_{\mathrm{i}}^{j}$, known as inelastic spatial velocity gradient of the corresponding Maxwell element and the inelastic rate of deformation tensor $\hat{\mathbf{D}}_{\mathrm{i}}^{(k)}$ is defined as:

$$\hat{\mathbf{L}}_{\mathrm{i}}^{(k)} = \dot{\hat{\mathbf{F}}}_{\mathrm{i}}^{(k)} \cdot \hat{\mathbf{F}}_{\mathrm{i}}^{-1(k)} \tag{13.12}$$

$$\hat{\mathbf{D}}_{\mathrm{i}}^{(k)} = \frac{1}{2}\left(\hat{\mathbf{L}}_{\mathrm{i}}^{(k)} + \hat{\mathbf{L}}_{\mathrm{i}}^{\mathrm{T}(k)}\right) \tag{13.13}$$

13.3.2.2 Derivation of the Potential Expressions

The free energy density $\rho_0\Psi$ for the considered case depends on the right Cauchy-Green deformation tensor $\mathbf{C}$, the elastic right Cauchy-Green deformation tensors $\hat{\mathbf{C}}_e^j$ and the thermodynamical temperature θ:

$$\rho_0\Psi = \rho_0\Psi\left(\mathbf{C}, \hat{\mathbf{C}}_{\mathrm{e}}^1, \ldots, \hat{\mathbf{C}}_{\mathrm{e}}^n, \theta\right) \tag{13.14}$$

Using the temporally free energy , the dissipation inequality (13.7) leads to:

$$\mathbf{S} : \frac{1}{2}\dot{\mathbf{C}} - \rho_0\left(2\frac{\partial\Psi}{\partial\mathbf{C}} : \frac{1}{2}\dot{\mathbf{C}} + \sum_{j=1}^{n}\frac{\partial\Psi}{\partial\hat{\mathbf{C}}_{\mathrm{e}}^j} : \dot{\hat{\mathbf{C}}}_{\mathrm{e}}^j + \frac{\partial\Psi}{\partial\theta}\dot{\theta}\right) - \rho_0\dot{\theta}\eta - \frac{\mathbf{q}_0}{\theta}\operatorname{Grad}\theta \geq 0 \tag{13.15}$$

The constitutive relations are obtained by fulfilling the Clausius-Duhem inequality (13.15). If Fourier's law is applied, the last term is non-negative, due to the negative proportionality between heat flux and temperature gradient,

$$\mathbf{q}_0 = -\lambda\mathbf{C}^{-1}\operatorname{Grad}\theta \qquad \text{with } \lambda \geq 0, \tag{13.16}$$

where λ is the heat conduction coefficient. After some transformations under consideration of the kinematic relations, one obtains the following inequality:

$$\begin{aligned}
&\left[\mathbf{S} - 2\rho_0\left(\frac{\partial\Psi}{\partial\mathbf{C}} + \sum_{j=1}^{n}(\det\mathbf{C})^{-\frac{1}{3}}\hat{\mathbf{F}}_{\mathrm{i}}^{j-1} \cdot \frac{\partial\Psi}{\partial\hat{\mathbf{C}}_{\mathrm{e}}^j} \cdot \hat{\mathbf{F}}_{\mathrm{i}}^{j-\mathrm{T}} - \sum_{j=1}^{n}\frac{1}{3}\left(\frac{\partial\Psi}{\partial\hat{\mathbf{C}}_{\mathrm{e}}^j} : \mathbf{I}\right)\mathbf{C}^{-1}\right)\right] : \frac{1}{2}\dot{\mathbf{C}} \\
&- \rho_0\left[\eta + \frac{\partial\Psi}{\partial\theta}\right]\dot{\theta} + 2\rho_0\sum_{j=1}^{n}\frac{\partial\Psi}{\partial\hat{\mathbf{C}}_{\mathrm{e}}^j} \cdot \hat{\mathbf{C}}_{\mathrm{e}}^{j\mathrm{T}} : \frac{1}{2}(\hat{\mathbf{L}}_{\mathrm{i}}^{j\mathrm{T}} + \hat{\mathbf{L}}_{\mathrm{i}}^{j}) \\
&+ \frac{\lambda}{\theta}(\operatorname{Grad}\theta) \cdot (\mathbf{C}^{-1}\operatorname{Grad}\theta) \geq 0
\end{aligned} \tag{13.17}$$

$\hat{\mathbf{L}}_{\mathrm{i}}^{j}$ is known as the inelastic spatial velocity gradient of the corresponding Maxwell element. The inequality is evaluated according to Coleman and Noll (1963). This means that each dependent variable is completely characterized by the values of the process variables and thus independent of their temporal changes. In addition, (13.17) has to be satisfied for arbitary values of $\dot{\theta}$ and tensors $\dot{\mathbf{C}}$. In this way, the constitutive equations can be obtained:

$$\mathbf{S} = 2\rho_0 \left(\frac{\partial \Psi}{\partial \mathbf{C}} + \sum_{j=1}^{n} (\det \mathbf{C})^{-\frac{1}{3}} \hat{\mathbf{F}}_{\mathrm{i}}^{j-1} \cdot \frac{\partial \Psi}{\partial \hat{\mathbf{C}}_{\mathrm{e}}^{j}} \cdot \hat{\mathbf{F}}_{\mathrm{i}}^{j-\mathrm{T}} - \sum_{j=1}^{n} \frac{1}{3} \left(\frac{\partial \Psi}{\partial \hat{\mathbf{C}}_{\mathrm{e}}^{j}} : \mathbf{I} \right) \cdot \mathbf{C}^{-1} \right) \tag{13.18}$$

$$\eta = -\frac{\partial \Psi}{\partial \theta} \tag{13.19}$$

To satisfy the residual inequality, proportionality relations with temperature-dependent functions $\breve{\eta}^{j}(\theta) \geq 0$ are introduced,

$$\hat{\mathbf{D}}_{\mathrm{i}}^{j} = \frac{2}{\breve{\eta}^{j}(\theta)} \frac{\partial \Psi}{\partial \hat{\mathbf{C}}_{\mathrm{e}}^{j}} \cdot \hat{\mathbf{C}}_{\mathrm{e}}^{j\mathrm{T}} \tag{13.20}$$

where $\hat{\mathbf{D}}_{\mathrm{i}}^{j}$ represents the symmetric part of the inelastic spatial velocity gradient. Furthermore, $\breve{\eta}^{j}(\theta)$ are interpreted as temperature-dependent viscosity functions, which are expressed by the standard Williams-Landel-Ferry equation (Williams et al, 1955):

$$\breve{\eta}^{j}(\theta) = \breve{\eta}_{t}^{j} \exp\left(-\frac{C_1(\theta - \theta_t)}{C_2 + \theta - \theta_t} \right) \tag{13.21}$$

In this context, $\breve{\eta}_{t}^{j}$ is the viscosity that belongs to the reference temperature θ_t and C_1, C_2 are empirical constants adjusted to fit the experimentally observed temperature dependence. Moreover, the deviatoric form of the evolution equation can be derived using the condition of incompressibility $(\det \hat{\mathbf{F}}_{\mathrm{i}})^{\cdot} = 0$. Taking into account the kinematic relations, the evolution equation can be reformulated as:

$$\dot{\hat{\mathbf{C}}}_{\mathrm{i}}^{j} = \hat{\mathbf{F}}_{\mathrm{i}}^{j\mathrm{T}} \cdot \left\{ \frac{2}{\breve{\eta}^{j}(\theta)} \frac{\partial \Psi}{\partial \hat{\mathbf{C}}_{\mathrm{e}}^{j}} \cdot \left[\hat{\mathbf{C}}_{\mathrm{e}}^{j\mathrm{T}} - \frac{1}{3} \mathrm{tr}\left(\hat{\mathbf{C}}_{\mathrm{e}}^{j\mathrm{T}} \right) \mathbf{I} \right] \right\} \cdot \hat{\mathbf{F}}_{\mathrm{i}}^{j} \tag{13.22}$$

Here, $\dot{\hat{\mathbf{C}}}_{\mathrm{i}}^{j}$ denotes the time derivative of the isochoric right Cauchy-Green deformation tensor related to the respective Maxwell element. The trace of a second order tensor is defined as $\mathrm{tr}(\circ) = (\circ) : \mathbf{I}$.

13.3.3 Heat Conduction Equation

From the first law of thermodynamics (13.4) in combination with the usage of the Legendre transform (13.6), one obtains:

$$\mathbf{S} : \frac{1}{2}\dot{\mathbf{C}} - \rho_0\left(\dot{\Psi} + \eta\dot{\theta}\right) - \rho_0\theta\dot{\eta} - \mathrm{Div}\left(\mathbf{q}_0\right) + \rho_0 r = 0 \tag{13.23}$$

Inserting the time derivative of the free energy density (13.14) leads to:

$$\rho_0\dot{\eta}\theta = \mathrm{Div}\left(\mathbf{q}_0\right) + \rho_0 r + 2\rho_0 \sum_{j=1}^{n} \frac{\partial \Psi}{\partial \hat{\mathbf{C}}_{\mathrm{e}}^{j}} \cdot \hat{\mathbf{C}}_{\mathrm{e}}^{j} : \hat{\mathbf{D}}_{\mathrm{i}}^{j} \tag{13.24}$$

In addition, the time derivative of the entropy density reads as:

$$\rho_0\dot{\eta} = \rho_0\left(\frac{\partial \eta}{\partial \theta}\dot{\theta} + \frac{\partial \eta}{\partial \mathbf{C}} : \dot{\mathbf{C}} + \sum_{j=1}^{n} \frac{\partial \eta}{\partial \hat{\mathbf{C}}_{\mathrm{e}}^{j}} : \dot{\hat{\mathbf{C}}}_{\mathrm{e}}^{j}\right) \tag{13.25}$$

Furthermore, the following simplifying assumption postulates a constant specific heat capacity c which is approximately equal to the isobaric specific heat capacity c_p:

$$c_p \approx c \approx -\frac{\partial \Psi}{\partial \theta \partial \theta}\theta \approx \mathrm{const} \tag{13.26}$$

Thus, the heat conduction equation is written in the current configuration as:

$$\rho\, c\, \dot{\theta} = -\,\mathrm{div}\left(\mathbf{q}\right) + \rho\, r + \rho\, \delta + \rho\, \pi \tag{13.27}$$

Here, $\mathbf{q}$ is the Cauchy heat flux vector with the associated operator $\mathrm{div}(\circ)$ that relates to the spatial coordinates. Furthermore, ρ is the density in the current configuration, $\rho\,\delta$ corresponds to the dissipation term and $\rho\,\pi$ represents the thermoelastic coupling term. Within the UMAT interface in the ABAQUS-software, these terms are added to the term ρr_{mat} such that the isobaric specific heat capacity remains on the left side (Abaqus, 2002).

$$\rho\, c_p\, \dot{\theta} = -\,\mathrm{div}\left(\mathbf{q}\right) + \rho\, r + \rho\, r_{mat} \tag{13.28}$$

13.4 Finite Element Implementation

After the formulation of the material model and the determination of the equations for the stress and entropy calculation, this section presents the material independent basic equations and methods for the implementation of the model in the commercial finite element software ABAQUS. Starting with the initial boundary value problem in the local form, the variation formulation is required for the approximate calculation. First, the required weak forms of the local quasi-static momentum balance and the heat conduction equation are presented and linearized for an iterative method. Here, it is focused on the constitutive equations and consistent tangent operators.

The balance equations (13.2) and (13.38) are general field equations for the determination of the displacement field $\mathbf{u}$ and the temperature θ. They are completed by the constitutive relations (13.18), (13.19). However, the determination of initial and

boundary conditions is mandatory for the unique description of the initial boundary value problem. From now on, quasi-static processes are considered whereby the initial conditions for the temperature field and the internal variables are required.

$$\theta(\mathbf{X}, t_0) = {}_{t=0}\theta(\mathbf{X}) \quad \text{and} \quad \hat{\mathbf{C}}_i^j(\mathbf{X}, t_0) = {}_{t=0}\hat{\mathbf{C}}_i^j(\mathbf{X}) \quad \text{for} \quad \mathbf{X} \in \Omega_0 \tag{13.29}$$

The specification of boundary conditions requires that the boundary $\partial\Omega_0$ of a body $\mathcal{B}_0$, which occupies the domain Ω_0, is divided into disjoint parts. The second subscript index indicates the type of boundary condition on the partial boundary, such that the following conditions are valid:

$$\partial\Omega_0 = \partial\Omega_{0u} \cup \partial\Omega_{0\sigma} \qquad \text{with} \qquad \partial\Omega_{0u} \cap \partial\Omega_{0\sigma} = \varnothing \tag{13.30}$$

$$\partial\Omega_0 = \partial\Omega_{0\theta} \cup \partial\Omega_{0q} \cup \partial\Omega_{0\theta q} \qquad \text{with} \qquad \partial\Omega_{0\theta} \cap \partial\Omega_{0q} \cap \partial\Omega_{0\theta q} = \varnothing \tag{13.31}$$

The Dirichlet boundary conditions are assigned to the values that a solution needs to take a long the boundary of the domain:

$$\mathbf{u}(\mathbf{X}, t) = \bar{\mathbf{u}}(\mathbf{X}, t) \text{ on } \partial\Omega_{0u} \quad \text{and} \quad \theta(\mathbf{X}, t) = \bar{\theta}(\mathbf{X}, t) \text{ on } \partial\Omega_{0\theta} \tag{13.32}$$

The Neumann boundary conditions are assigned to the values in which the derivative of a solution is applied with

$$\mathbf{q}_0 \cdot \mathbf{n}_0 = \bar{q}_0(\mathbf{X}, t) \text{ on } \partial\Omega_{0q} \quad \text{and} \quad \mathbf{t}_0 = \mathbf{P}\mathbf{n}_0 = \bar{\mathbf{t}}_0(\mathbf{X}, t) \text{ on } \partial\Omega_{0\sigma}. \tag{13.33}$$

The mixed boundary surfaces, where the condition additionally dependents on the surface temperature

$$\mathbf{q}_0 \cdot \mathbf{n}_0 = \bar{q}_0(\mathbf{X}, t, \theta) \text{ on } \partial\Omega_{0\theta q} \tag{13.34}$$

is specified. This results in a well-defined initial boundary value problem. The operator $(\bar{\circ})$ denotes a prescribed function on the boundary where $\mathbf{n}_0$ is the outward normal to the boundary $\partial\Omega_0$ and $\mathbf{t}_0$ depicts the first Piola-Kirchhoff traction vector which is associated to the reference configuration. An analytical solution of the field problem is usually not possible. However, an approximate solution can be calculated using the finite element method exemplary. This requires the formulation of balance equations in the form of variational principles.

The weak formulation of the problem is mandatory for the finite element implementation. Therefore, the balance of linear momentum (13.2) has to be rearranged in terms of quantities which are related to the current configuration first. Secondly, it is assumed that the acceleration is zero for quasi-static processes. This leads to the spatial quasi-static balance of momentum.

$$\operatorname{div} \boldsymbol{\sigma} + \rho\mathbf{b} = \mathbf{0} \tag{13.35}$$

As the next steps to derive the weak formulation. The balance equation is multiplied with the test function $\delta\mathbf{v}$ and integrated over the area Ω where $\delta\mathbf{v}$ is the first variation of the spatial velocity vector. Using the Gaussian integral theorem and the boundary condition (13.33) provides the weak form of mechanical equilibrium as a

mechanical functional $\mathcal{M}$, where the gradient operator grad$(\circ)$ corresponds to the current configuration.

$$\mathcal{M}(\mathbf{u},\theta,\delta\mathbf{v}) = \int_{\Omega} \boldsymbol{\sigma} : \operatorname{grad}\delta\mathbf{v}\,\mathrm{d}V - \int_{\partial\Omega_{\sigma}} \bar{\mathbf{t}}\cdot\delta\mathbf{v}\,\mathrm{d}A - \int_{\Omega} \rho\mathbf{b}\cdot\delta\mathbf{v}\,\mathrm{d}V = 0 \tag{13.36}$$

To obtain the variation formulation of the heat conduction equation, the heat conduction equation (13.28) is multiplied by the variation of the temperature $\delta\theta$. The thermal functional $\mathcal{T}$ follows from the subsequent reformulation and insertion of the boundary condition (13.34):

$$\begin{aligned}\mathcal{T}(\mathbf{u},\theta,\delta\theta) = \int_{\Omega} \rho c_p\dot{\theta}\delta\theta\mathrm{d}V - \int_{\partial\Omega_q} \bar{q}_0\delta\theta\mathrm{d}A \\ + \int_{\Omega} \mathbf{q}\cdot\operatorname{grad}\delta\theta\mathrm{d}V + \int_{\Omega} \rho(r+r_{mat})\delta\theta\mathrm{d}V = 0\end{aligned} \tag{13.37}$$

In the following, the thermomechanical problem is formulated. Both functionals (13.36) and (13.37) have to be fulfilled. The two requirements are combined with weighting factors to get a fully coupled functional $\mathcal{G}$, such that a closed solution is achieved.

$$\begin{aligned}\mathcal{G} &= \mathcal{M}_u\mathcal{M} + \mathcal{T}_\theta\mathcal{T} \\ &= \mathcal{M}_u\left\{\int_{\Omega} \boldsymbol{\sigma} : \operatorname{grad}\delta\mathbf{v}\,\mathrm{d}V - \int_{\partial\Omega_{\sigma}} \bar{\mathbf{t}}\cdot\delta\mathbf{v}\,\mathrm{d}A - \int_{\Omega} \rho\mathbf{b}\cdot\delta\mathbf{v}\,\mathrm{d}V\right\} \\ &+ \mathcal{T}_\theta\left\{\int_{\Omega} \rho c_p\dot{\theta}\delta\theta\mathrm{d}V - \int_{\partial\Omega_q} \bar{q}_0\delta\theta\mathrm{d}A + \int_{\Omega} \mathbf{q}\cdot\operatorname{grad}\delta\theta\mathrm{d}V + \int_{\Omega} \rho(r+r_{mat})\delta\theta\mathrm{d}V\right\}\end{aligned} \tag{13.38}$$

Since the functionals are non-linear in temperature and displacement, further considerations are necessary. To solve nonlinear functions, they have to be linearized, e.g. with the Gâteux derivative:

$$\mathcal{D}_{\Delta u}(\circ(\mathbf{x})) = \mathcal{D}_u(\circ(\mathbf{x}))\Delta\mathbf{u} = \Delta(\circ) = \frac{\mathrm{d}}{\mathrm{d}\epsilon}(\circ(\mathbf{x}+\epsilon\boldsymbol{\Delta}\mathbf{u}))\Big|_{\epsilon=0} \tag{13.39}$$

The subscript $\mathcal{D}_{(\circ)}$ indicates the direction of the linearization. Thus, the solution at time t_k can be determined iteratively from the solution at the time t_{k-1}, for example with the Newton method. For the i-th iteration step at time $t = t_k$ the notation ${}^{i}_{k}(\circ)$ is introduced. The temperature velocity occurring in the thermal functional (13.37) is approximated from the time discretization with the Euler backward method.

$${}^{i}_{k}\dot{\theta} = \frac{{}^{i}_{k}\theta - {}_{k-1}\theta}{\Delta t} \tag{13.40}$$

Then, one obtains the linearized functional in the form

$$D\mathcal{M}({}^{i+1}_{k}\mathbf{u}, {}^{i+1}_{k}\theta, \delta\mathbf{v}) = \mathcal{M}({}^{i}_{k}\mathbf{u}, {}^{i}_{k}\theta, \delta\mathbf{v}) + D_u\mathcal{M}({}^{i}_{k}\mathbf{u}, {}^{i}_{k}\theta, \delta\mathbf{v})\Delta\mathbf{u} + D_\theta\mathcal{M}({}^{i}_{k}\mathbf{u}, {}^{i}_{k}\theta, \delta\mathbf{v})\Delta\theta = 0 \tag{13.41}$$

$$D\mathcal{T}({}^{i+1}_{k}\mathbf{u}, {}^{i+1}_{k}\theta, \delta\theta) = \mathcal{T}({}^{i}_{k}\mathbf{u}, {}^{i}_{k}\theta, \delta\theta) + D_u\mathcal{T}({}^{i}_{k}\mathbf{u}, {}^{i}_{k}\theta, \delta\theta)\Delta\mathbf{u} + D_\theta\mathcal{T}({}^{i}_{k}\mathbf{u}, {}^{i}_{k}\theta, \delta\theta)\Delta\theta = 0 \tag{13.42}$$

or simplified in matrix notation:

$$\begin{pmatrix} D_u\mathcal{M} & D_\theta\mathcal{M} \\ D_u\mathcal{T} & D_\theta\mathcal{T} \end{pmatrix} \begin{pmatrix} \Delta\mathbf{u} \\ \Delta\theta \end{pmatrix} = \begin{pmatrix} -\mathcal{M} \\ -\mathcal{T} \end{pmatrix} \tag{13.43}$$

The implementation of the material model requires the calculation of the state vector and the definition of the state vector dependent contribution to the tangent stiffness matrix. Therefore, the linearization of the terms δP_{int} and δK_{mat} are of special importance and defined as follows:

$$\delta P_{\text{int}} = \int_\Omega \boldsymbol{\sigma} : \operatorname{grad}\delta\mathbf{v}\, \mathrm{d}V, \qquad \delta K_{\text{mat}} = \int_\Omega \delta\theta\rho r_{mat}\, \mathrm{d}V \tag{13.44}$$

The linearization of the mechanical part (13.36) in the direction of the incremental displacement field $\Delta\mathbf{u}$ leads to the mechanical contribution of the tangent stiffness matrix follows:

$$D_{\Delta u}\delta P_{\text{int}} = \int_\Omega [\delta\mathbf{D} : \overset{\triangledown}{\mathbb{C}} : \Delta\mathbf{D} + \delta\mathbf{D} : \Delta\mathbf{W}\boldsymbol{\sigma} - \delta\mathbf{D} : \boldsymbol{\sigma}\Delta\mathbf{W}]\, \mathrm{d}V \tag{13.45}$$

The additive decomposition of the spatial velocity gradient $\mathbf{L}$ contains a symmetric part known as rate of deformation tensor and the antisymmetric part, the spin tensor, denoted as $\mathbf{D}$ and $\mathbf{W}$, follows respectively. The objective spatial tangent operator has to be implemented in the Jaumann formulation $\overset{\triangledown}{\mathbb{C}}$. This includes the rotated parts of the stress and the spatial tangent operator $\overset{4}{\mathbb{c}}$, which can be calculated from the material tangent operator $\overset{4}{\mathbb{C}}$. The transposition of the indices is defined as $[(\circ)]^{\overset{ij}{\mathrm{T}}} = (\circ)_{ijkl}\mathbf{e}_j \otimes \mathbf{e}_i \otimes \mathbf{e}_k \otimes \mathbf{e}_l$. The definition of the required tangent operator is shown as follows:

$$\overset{\triangledown}{\mathbb{C}} = \frac{1}{J}\overset{4}{\mathbb{C}} + \left[\mathbf{I} \otimes \boldsymbol{\sigma}\right]^{\overset{23}{\mathrm{T}}} + \left[\boldsymbol{\sigma} \otimes \mathbf{I}\right]^{\overset{23}{\mathrm{T}}} \tag{13.46}$$

$$\overset{4}{\mathbb{c}} = \left[\mathbf{F} \otimes \mathbf{F}\right]^{\overset{23}{\mathrm{T}}} : \overset{4}{\mathbb{C}} : \left[\mathbf{F}^{\mathrm{T}} \otimes \mathbf{F}^{\mathrm{T}}\right]^{\overset{23}{\mathrm{T}}} \qquad \text{with} \qquad \overset{4}{\mathbb{C}} = 4\rho_0 \frac{\partial^2\Psi}{\partial\mathbf{C}\partial\mathbf{C}} \tag{13.47}$$

After the mechanical part (13.36) is linearized in the direction of $\Delta\theta$, the mechanical-thermal contribution is obtained:

$$D_{\Delta\theta}\delta P_{\text{int}} = \int_{\Omega} \delta\mathbf{D} : \mathbf{t}^{\theta}\Delta\theta \, \mathrm{d}V \tag{13.48}$$

It contains The spatial mechanical-thermo coupling tangent to be implemented in the form of the stress temperature tensor $\mathbf{t}^{\theta}$:

$$\mathbf{t}^{\theta} = \frac{2}{J}\rho_0\mathbf{F} \cdot \frac{\partial^2\Psi}{\partial\theta\partial\mathbf{C}} \cdot \mathbf{F}^{\mathrm{T}} \tag{13.49}$$

The same procedure is applied to the thermal component. The thermo-mechanical contribution is expressed by

$$D_{\Delta\theta}\delta K_{\text{mat}} = \int_{\Omega} \delta\theta\mathbf{d}^{\mathbf{u}} : \Delta\mathbf{D} \, \mathrm{d}V \tag{13.50}$$

with the following definition of the thermo-mechanical coupling tangent $\mathbf{d}^{\mathbf{u}}$ with respect to spatial coordinates

$$\mathbf{d}^{\mathbf{u}} = \frac{2}{J}\rho_0\mathbf{F} \cdot \frac{\partial r_{mat}}{\partial\mathbf{C}} \cdot \mathbf{F}^{\mathrm{T}} \tag{13.51}$$

and finally the thermal contribution is:

$$D_{\Delta\theta}\delta K_{\text{mat}} = \int_{\Omega} \delta\theta d^{\theta}\Delta\theta \, \mathrm{d}V \tag{13.52}$$

Accordingly, the thermal tangent operator is calculated as:

$$d^{\theta} = \frac{1}{J}\rho_0\frac{\partial r_{mat}}{\partial\theta} \tag{13.53}$$

13.5 Material Model

The linearization leads to the definition of the material independent tangent operators (13.46), (13.49), (13.51), (13.53) which are mandatory besides the state vector in order to solve the fully coupled problem. Since elastomers behave almost incompressible under isothermal deformations, a volumetric-isochoric separation is advantageous. Furthermore, the isochoric part of the elastic Cauchy-Green tensor is introduced as a variable in the isochoric part of the free energy density. There are also different approaches for the determination of the thermal part of the free energy. The total free energy is calculated as follows:

$$\rho_0\Psi\left(I_{\hat{\mathbf{C}}}, II_{\hat{\mathbf{C}}}, I_{\hat{\mathbf{C}}_{\mathrm{e}}^j}, J, \theta\right) = \rho_0\Psi_{\text{th}}(\theta) + \rho_0\Psi_{\text{vol}}\left(J\right) \tag{13.54}$$

$$+ \rho_0 \Psi_{\mathrm{eq}}\left(I_{\hat{\mathbf{C}}}, II_{\hat{\mathbf{C}}}\right) + \sum_{j=1}^{n} \rho_0 \Psi_{\mathrm{neq}}^{j}\left(I_{\hat{\mathbf{C}}_{\mathrm{e}}^{j}}\right)$$

In various studies, the temperature-dependent part is specified by the requirement of a constant heat capacity at a constant deformation. Here, the following approach is chosen for thus thermal part of the free energy density (Holzapfel, 2000):

$$\rho_0 \Psi_{\mathrm{th}}(\theta) = \rho_0 c \left(\left(\theta - \theta_0\right) - \theta \ln \frac{\theta}{\theta_0} \right) \tag{13.55}$$

The incompressible material behaviour must be taken into account in the stress calculation, which can lead to numerical difficulties. The volumetric approaches usually use the determinant of the deformation gradient as independent variable (Simo and Taylor, 1982) :

$$\rho_0 \Psi_{\mathrm{vol}}\left(J\right) = \frac{1}{2} \kappa \left[\left(J - 1\right)^2 + \left(\ln J\right)^2 \right] \tag{13.56}$$

where, the material parameter κ has the function of a penalty parameter. In the literature, a number of approaches for the isochoric part of the free energy density can be found e.g. Mooney (1940); Rivlin (1948-1951) or Rivlin (1997). They use the invariants of the Cauchy-Green tensors $I_{\square}$ and $II_{\square}$ as variables.

The equilibrium part of the free energy density reads as follows (Mooney, 1940):

$$\rho_0 \Psi_{\mathrm{eq}}\left(I_{\hat{\mathbf{C}}}, II_{\hat{\mathbf{C}}}\right) = C_{10}\left(I_{\hat{\mathbf{C}}} - 3\right) + C_{20}\left(I_{\hat{\mathbf{C}}} - 3\right)^2 + C_{01}\left(II_{\hat{\mathbf{C}}} - 3\right) \tag{13.57}$$

The non-equilibrium parts of the free energy density (Mooney, 1940) are assumed as:

$$\sum_{j=1}^{n} \rho_0 \Psi_{\mathrm{neq}}^{j}\left(I_{\hat{\mathbf{C}}_{\mathrm{e}}^{j}}\right) = \sum_{j=1}^{n} C_{\mathrm{e}10}^{j}\left(I_{\hat{\mathbf{C}}_{\mathrm{e}}^{j}} - 3\right) \tag{13.58}$$

Where the material parameters $C_{10}, C_{20}, C_{01}, C_{\mathrm{e}10}^{1}, ..., C_{\mathrm{e}10}^{n}$ are temperature independent and therefore constant. In the following, the free energy densities are used to describe stresses, heat sources and internal variables. In addition to that, tangent operators for the mechanical, thermal and coupling behaviour, are presented.

The internal variables are described by the evolution equations (13.22). Using (13.58), they can be solved numerically according to a method proposed by Shutov et al (2013) and expressed further by the isochoric elastic left Cauchy-Green tensor $\hat{\mathbf{B}}_e = \hat{\mathbf{F}} \cdot \hat{\mathbf{C}}_{\mathrm{i}}^{-1} \cdot \hat{\mathbf{F}}^{\mathrm{T}}$:

$$\dot{\hat{\mathbf{C}}}_i^j = \frac{4 C_{e10}^j}{\breve{\eta}^j(\theta)} \left[\hat{\mathbf{C}} - \frac{1}{3} \operatorname{tr}\left(\hat{\mathbf{C}} \cdot \hat{\mathbf{C}}_i^{j-1} \right) \hat{\mathbf{C}}_i^j \right] \tag{13.59}$$

Inserting the free energy densities (13.56)-(13.58) into the stress definition (13.18) and transforming the quantities to the current configuration, the Cauchy stress is

obtained:

$$\boldsymbol{\sigma} = \boldsymbol{\sigma}_{vol} + \boldsymbol{\sigma}_{eq} + \sum_{j=1}^{n} \boldsymbol{\sigma}_{neq}^{j} \tag{13.60}$$

The volumetric part of Cauchy stress is:

$$\boldsymbol{\sigma}_{vol} = J^{-1}\kappa\Big(J\big(J-1\big) + \ln J\Big)\mathbf{I} \tag{13.61}$$

The equilibrium part of Cauchy stress is:

$$\begin{aligned}\boldsymbol{\sigma}_{eq} = \frac{2}{J}\Big[&\Big(C_{10} + 2C_{20}\big(I_{\hat{\mathbf{B}}} - 3\big) + C_{01}I_{\hat{\mathbf{B}}}\Big)\hat{\mathbf{B}} - C_{01}\hat{\mathbf{B}}^2 \\ &-\frac{1}{3}\Big(I_{\hat{\mathbf{B}}}\big(C_{10} + 2C_{20}(I_{\hat{\mathbf{B}}} - 3)\big) + 2C_{01}II_{\hat{\mathbf{B}}}\Big)\mathbf{I}\Big]\end{aligned} \tag{13.62}$$

The non-equilibrium part of the Cauchy stress is:

$$\boldsymbol{\sigma}_{neq} = \sum_{j=1}^{n} C_{e10}^{j}\big(I_{\hat{\mathbf{B}}_e^j} - 3\big) \tag{13.63}$$

The inelastic stress power is represented by variables of the current configuration:

$$r_{mat} = \sum_{j=1}^{n} \frac{1}{\check{\eta}^{j}(\theta)}\boldsymbol{\sigma}_{neq}^{j} : \boldsymbol{\sigma}_{neq}^{j} \tag{13.64}$$

Using the equation (13.47) and (13.56)-(13.58) yields to the tangent of the current configuration

$$\overset{4}{\mathbb{C}} = \overset{4}{\mathbb{C}}_{vol} + \overset{4}{\mathbb{C}}_{eq} + \sum_{j=1}^{n} \overset{4}{\mathbb{C}}_{neq}^{j} \tag{13.65}$$

The volumetric part of the tangent is:

$$\overset{4}{\mathbb{C}}_{vol} = \frac{1}{J}\Big[\kappa\Big(J\big(2J-1\big)+1\Big)\Big[\mathbf{I}\otimes\mathbf{I}\Big] + 2\kappa\Big(J\big(1-J\big) - \ln J\Big)\Big[\mathbf{I}\otimes\mathbf{I}\Big]^{\overset{23}{\mathrm{T}}}\Big] \tag{13.66}$$

The equilibrium part of the tangent is:

$$
\begin{aligned}
\overset{4}{\mathbb{C}}_{eq} = \frac{4}{3J}\Big[& -\Big(C_{10} + 2C_{20}\big(I_{\hat{\mathbf{B}}} - 3\big) + 2I_{\hat{\mathbf{B}}}\big(C_{20} + C_{01}\big)\Big)\Big[\mathbf{I}\otimes\hat{\mathbf{B}} + \hat{\mathbf{B}}\otimes\mathbf{I}\Big] \\
& + \Big(2C_{20} + C_{01}\Big)\Big[\hat{\mathbf{B}}\otimes\hat{\mathbf{B}}\Big] \\
& + \frac{2}{3}C_{01}\Big[\mathbf{I}\otimes\hat{\mathbf{B}}^2 + \hat{\mathbf{B}}^2\otimes\mathbf{I}\Big] \\
& + C_{01}\Big[\hat{\mathbf{B}}\otimes\hat{\mathbf{B}}\Big]^{\overset{23}{\mathrm{T}}} \\
& + \frac{1}{9}\Big(I_{\hat{\mathbf{C}}}\big(C_{10} + 2C_{20}\big(I_{\hat{\mathbf{C}}} - 3\big) + 2C_{20}I_{\hat{\mathbf{C}}}\big) + 4C_{01}II_{\hat{\mathbf{C}}}\Big)\Big[\mathbf{I}\otimes\mathbf{I}\Big] \\
& + \frac{1}{3}\Big(I_{\hat{\mathbf{C}}}\Big(C_{10} + 2C_{20}\big(I_{\hat{\mathbf{C}}} - 3\big)\Big) + 2C_{01}II_{\hat{\mathbf{C}}}\Big)\Big[\mathbf{I}\otimes\mathbf{I}\Big]^{\overset{23}{\mathrm{T}}}\Big]
\end{aligned}
\tag{13.67}
$$

Non-equilibrium part of the tangent:

$$
\overset{4}{\mathbb{C}}_{neq} = \sum_{j=1}^{n}\frac{4}{3J}C^{j}_{e10}\Big[\operatorname{tr}\big(\hat{\mathbf{B}}^{j}_{e}\big)\Big[\frac{1}{3}\mathbf{I}\otimes\mathbf{I} + \Big[\mathbf{I}\otimes\mathbf{I}\Big]^{\overset{23}{\mathrm{T}}}\Big] - \Big[\hat{\mathbf{B}}^{j}_{e}\otimes\mathbf{I} + \mathbf{I}\otimes\hat{\mathbf{B}}^{j}_{e}\Big]\Big] \tag{13.68}
$$

The remaining tangents of the current configuration are formulated by definitions (13.49), (13.51), (13.53) derived in the previous section. The stress temperature tensor is zero:

$$
\mathbf{t}^{\theta} = \mathbf{0} \tag{13.69}
$$

The thermal-mechanical tangent is:

$$
\mathbf{d}^{\mathbf{u}} = \sum_{j=1}^{n}\frac{4}{\breve{\eta}^{j}(\theta)}\,\boldsymbol{\sigma}^{j}_{neq}\cdot\Big(J\,\boldsymbol{\sigma}^{j}_{neq} - \frac{1}{3}\operatorname{tr}\big(J\,\boldsymbol{\sigma}^{j}_{neq}\big)\mathbf{I}\Big) \tag{13.70}
$$

The thermal tangent is:

$$
d^{\theta} = \sum_{j=1}^{n}\frac{\breve{\eta}^{j}(\theta)^{-2}}{J}\frac{C_1\,C_2\,\breve{\eta}^{j}_{t}\exp(-\frac{C_1(\theta-\theta_t)}{C_2+\theta-\theta_t})}{\big(-C_2-(\theta-\theta_t)\big)^2}\boldsymbol{\sigma}^{j}_{neq}:\boldsymbol{\sigma}^{j}_{neq} \tag{13.71}
$$

The last step is to formulate the required quantities in the Voigt notation. To this end, it is essential to symmetrize the tensors if necessary. Now, all tangent operators (13.46), (13.69), (13.70), (13.71) and state vectors (13.58) and (13.64) required for the fully coupled calculation are defined correctly.

13.6 Model Validation

The material model is validated as discussed in this section. First, the derivation of the parameter set is explained. Secondly, the structure of the calculation of the

model is explained as well as the derivation of the boundary and initial conditions. With these definitions, the simulation results are compared with the experimentally determined data.

13.6.1 Parameter Identification

First, the parameter Set used for the current model is listed in Table 13.1. With the exceptions explained below, these are all independently determined parameters. One characteristic of the parameter set is that the compression modulus κ is chosen at least three orders higher than the shear modulus in order to formulate the quasi-incompressible material behaviour and thus is used as a penalty parameter. Furthermore, the optimized heat capacity c_p^{opt} is of particular importance. The integration of the heat conduction equation with respect to the current configuration over a period of time T in the stationary range shows the independence of the stationary state from the heat capacity c_p. Where $\vartheta(\mathbf{X},t)$ is a scalar temperature field depending on the location coordinate and time. Regarding the left side of the term, one can conclude that:

Table 13.1 Parameter set used for the modified finite strain thermo-viscoelastic material model

parameter	value	unit
Quasi-incompressible hyperelasticity: Mooney-RivlinMooney (1940)		
C_{10}	0.0788	MPa
C_{20}	0.0107	MPa
C_{01}	0.1739	MPa
ρ_0	$1.0748 \cdot 10^{-9}$	kg/m^3
κ	1000	MPa
viscoelasticity: Neo-HookeMooney (1940)		
C^1_{e10}	0.0042	MPa
$\check{\eta}^1_t$	0.005	MPas
C^2_{e10}	0.1020	MPa
$\check{\eta}^2_t$	0.1201	MPas
temperature dependence $\check{\eta}^j(\theta)$, Williams, Landel, FerryWilliams et al (1955)		
C_1	-16	-
C_2	-730	K
θ_t	296	K
thermal material properties		
λ	0.3280	mW/K $\cdot$ mm
c_p	$1.639 \cdot 10^9$	mJ/t $\cdot$ K
c_p^{opt}	$1.639 \cdot 10^7$	mJ/t $\cdot$ K
heat transfer		
$\check{\alpha}^{ES}$	$22 \cdot 10^{-3}$	mW/mm^2 $\cdot$ K
$\check{\alpha}^{EA}$	$5 \cdot 10^{-3}$	mW/mm^2 $\cdot$ K

$$\frac{1}{T}\int_{t}^{t+T} \rho c_p \dot{\vartheta}(s)\mathrm{d}s = \rho c_p \Big(\vartheta(t+T) - \vartheta(t)\Big) = 0. \tag{13.72}$$

This motivates to the usage of an optimized heat capacity to reduce the calculation time to reach the stationary state. Finally, the heat transfer coefficients from elastomer to air $\breve{\alpha}^{EA}$ is calculated from Stephan (2002) and that from elastomer to steel $\breve{\alpha}^{ES}$ is taken from Schlanger (1983) or Klauke (2015).

13.6.2 Computational Model

For the computational model (Fig. 13.3), the formulation of the boundary conditions is mandatory. This section describes the boundary condition formulation as shown in Fig. 13.3. For the mixed boundary conditions, the heat transfers from the elastomer to the ambient air and from the elastomer to the steel are defined as heat flows $\mathbf{q}_0^{\mathrm{EA}} = -\breve{\alpha}^{\mathrm{EA}}(\theta_{\partial\Omega} - \theta_{\mathrm{t}})$ and $\mathbf{q}_0^{\mathrm{ES}} = -\breve{\alpha}^{\mathrm{ES}}(\theta_{\partial\Omega} - \theta_{\mathrm{t}})$, respectivley. In addition, the displacement boundary conditions are defined in the form $\bar{\mathbf{u}}_0^{\mathrm{FIX}} = \mathbf{0}$ for the fixed constraint and $\bar{\mathbf{u}}_0^{\mathrm{SYMX}} = [0\, u_2\, u_3]^{\mathrm{T}}$ or $\bar{\mathbf{u}}_0^{\mathrm{SYMY}} = [u_1\, 0\, u_3]^{\mathrm{T}}$ for the symmetry constraint. The force is applied at the reference point P_{REF} by $\mathbf{f} = [F_0 \sin(\omega t)\, 0\, 0]$ where $F_0 = 1.4/4$ [kN] and $\omega = 4\pi$ [1/s]. This results in a completely thermomechanically coupled problem.

13.6.3 Analysis

The simulation results are now compared to the experimental data. Multiple experiments were carried out as part of the so-called Elasto-Opt II project at the Fraunhofer LBF in Darmstadt (Schröder and Parra Pelaez, 2019). First, the force-displacement curve at the reference point is considered and shown in Fig. 13.4 (right). A nearly

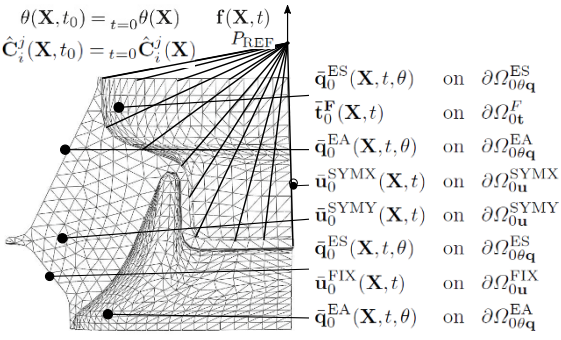

Fig. 13.3 Computational model showing mixed boundary conditions and displacement boundary conditions as well as fixed and symmetry constraints

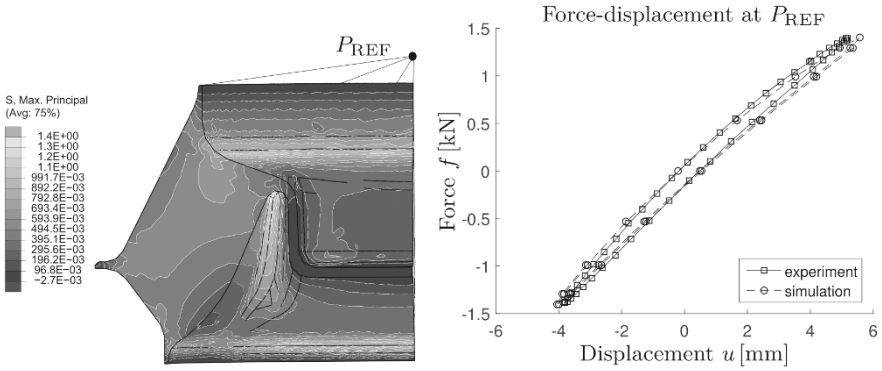

Fig. 13.4 Local stresses on the engine bearing (left). Force-displacement hysteresis of the engine bearing at the reference point (right)

identical hysteresis is observed. This means that in addition to the mechanical i.e. the force-displacement, behaviour, the dissipative behaviour, which is characterized by the hysteresis area, is also mapped. Accordingly, the local loads can be deduced at this point as shown in Figure 13.4.
The self-heating caused by dissipation is shown in Fig. 13.5. The surface temperatures were experimentally determined using an infrared camera technology. For reasons of clarity, the experimental data smoothed. This was performed with the calculated temperature curve. In Fig. 13.5 (right), the agreement of the stationary temperature values can be recognized. However, it is observed that the calculation duration is significantly reduced by the suitable selection of the heat capacity. Furthermore, the local temperature profile in the stationary state can be inferred. In consequence, a temperature rise of approximately 18 K can be observed under the given conditions. The point in time at which the stationary temperature equilibrium is reached is marked

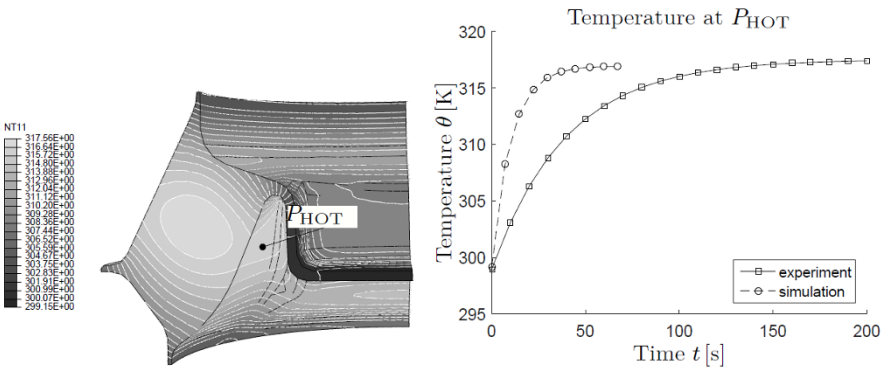

Fig. 13.5 Local temperature distribution in the engine bearing (left). Temperature evolution with respect to the time of the engine bearing at the hotspot (right)

with τ_s. Using this variable, the time-dependent temperature curves are now described. At this point it is also interesting to compute temperature curves which are difficult to measure. In particular, the thickest component cross-section is considered here. The path defined on the finite element mesh is used to evaluate the temporal temperature curve as shown in Fig. 13.6. Finally, the simulation shows a high concordance to the experimental data under consideration of an efficient simulation methodology.

13.7 Summary and Conclusion

In this work, a calculation concept for the estimation of the change in local component temperatures caused by dissipative heating was presented. Based on the phenomenological consideration of elastomer materials, phenomena relevant to self-heating were identified and used as a basis for the constitutive modelling. A modified model of the finite thermoviscoelasticity was continuum mechanically modelled. In addition to the kinematic description, a thermomechanically consistent derivation of the constitutive relations as well as the formulation of the heat conduction equation was performed. Within the framework of finite element implementation, the unique initial and boundary value problem was presented and a fully coupled functional was derived using the variation principle. The tangent operators were subsequently determined by linerisation. A special approach of the total free energy density was defined and used for the analytical calculation of state vectors and consistent tangent operators. Finally, the model was validated, starting with the explanation of the parameterisation and model calculations, followed by comparison of experiments and simulations as well as their discussion. Last but not least, not only the experimental setup but also the calculation effort can be significantly reduced compared to the classical model of finite thermal viscoelasticity by neglecting the thermoelastic effects. In summary, it can be said that the implemented concept is a suitable instrument for the

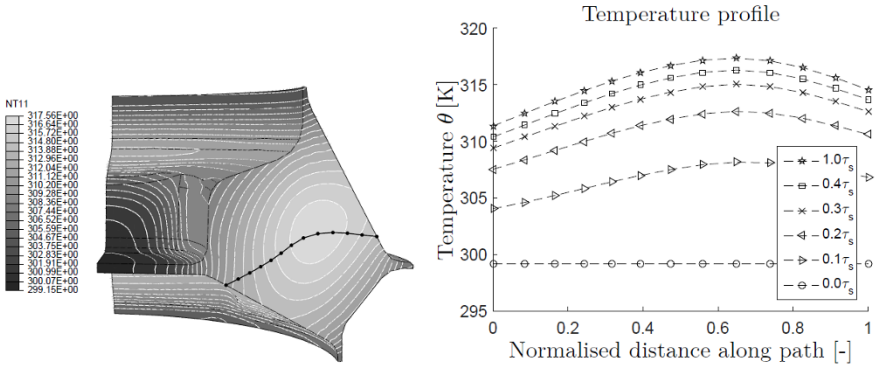

Fig. 13.6 Local temperature distribution in the engine bearing (left). Temperature evolution with respect to the time of the engine bearing at the path (right)

robust, cost-effective and valid estimation of dissipation-related temperature changes in components. In the future, characteristic diagrams of the stationary component temperatures over large amplitude and frequency ranges should be created with this methodology. The necessity of the experimental determination of a parameter or the use of literature data shall be determined by means of a parameter analysis. Furthermore, of different components and elastomer compounds may be validated as part of a follow-up project.

References

Abaqus (2002) ABAQUS/CAE 6.14 User's Manual. Hibbitt, Karlsson & Sorensen, Incorporated

Anand L (1985) Constitutive equations for hot-working of metals. International Journal of Plasticity 1(3):213–231

Anand L, Ames NM, Srivastava V, Chester SA (2009) A thermo-mechanically coupled theory for large deformations of amorphous polymers. part i: Formulation. International Journal of Plasticity 25(8):1474–1494

Anthony RL, Caston RH, Guth E (1942) Equations of state for natural and synthetic rubber-like materials. i. unaccelerated natural soft rubber. The Journal of Physical Chemistry 46(8):826–840

Arruda EM, Boyce MC, Jayachandran R (1995) Effects of strain rate, temperature and thermomechanical coupling on the finite strain deformation of glassy polymers. Mechanics of Materials 19(2-3):193–212

Bröcker C (2013) Materialmodellierung für die simultane Kalt-/Warmumformung auf Basis erweiterter rheologischer Modelle. kassel university press GmbH

Bröcker C, Matzenmiller A (2008) Modellierung und simulation thermo-mechanisch gekoppelter umformprozesse. In: Proceedings in Applied Mathematics and Mechanics, Wiley Online Library, vol 8, pp 10,485–10,486

Coleman BD, Noll W (1963) The thermodynamics of elastic materials with heat conduction and viscosity. Archive for Rational Mechanics and Analysis 13:167–178

Dippel B, Johlitz M, Lion A (2014) Thermo-mechanical couplings in elastomers - experiments and modelling. Journal of Applied Mathematics and Mechanics doi:10.1002/zamm.201400110

Elsner P, Eyerer P, Hirth T (2012) Domininghaus - Kunststoffe: Eigenschaften und Anwendungen. VDI-Buch, Springer Berlin Heidelberg

Erbts P, DüSter A (2012) Accelerated staggered coupling schemes for problems of thermoelasticity at finite strains. Computers & Mathematics with Applications 64(8):2408–2430

Flory PJ (1961) Thermodynamic relations for high elastic materials. Transactions of the Faraday Society 57:829–838

Glaser S (1992) Berechnung gekoppelter thermomechanischer Prozesse. Dissertation, Institut für Baumechanik und Numerische Mechanik, Universität Hannover, Bericht-Nr. F88/6

Gough J (1805) A description of a property of caoutchouc, or indian rubber. Memories of the Literacy and Philosophical Society of Manchester 1:288–295

Hamkar AW (2013) Eine iterationsfreie Finite-Elemente Methode im Rahmen der finiten Thermoviskoelastizität. Universitätsbibliothek Clausthal

Heimes T (2004) Finite Thermoviskoelastizität. Forschungs- und Seminarbericht aus dem Gebiet Technische Mechanik und Flächentragwerke, Universität der Bundeswehr München

Holzapfel GA (2000) Nonlinear Solid Mechanics: A Continuum Approach for Engineering Science. Wiley

Johlitz M (2015) Zum Alterungsverhalten von Polymeren: Experimentell gestützte, thermochemomechanische Modellbildung und numerische Simulation. Habilitationsschrift Institut für Mechanik an der Universität der Bundeswehr München

Joule JP (1859) On some thermo-dynamic properties of solids. Philosophical Transactions of the Royal Society of London 149:91–131
Klauke R (2015) Lebensdauervorhersage mehrachsig belasteter Elastomerbauteile unter besonderer Berücksichtigung rotierender Beanspruchungsrichtungen. Fakultät für Maschinenbau der Technischen Universität Chemnitz, Institut für Mechanik und Thermodynamik
Koltzenburg S, Maskos M, Nuyken O (2013) Polymere: Synthese, Eigenschaften und Anwendungen. Springer-Verlag
Lejeunes S, Eyheramendy D, Boukamel A, Delattre A, Méo S, Ahose KD (2018) A constitutive multiphysics modeling for nearly incompressible dissipative materials: application to thermo–chemo-mechanical aging of rubbers. Mechanics of Time-Dependent Materials 22(1):51–66
Lion A (2000) Thermomechanik von Elastomeren. Berichte des Instituts für Mechanik der Universität Kassel (Bericht 1/2000)
Lubliner J (1985) A model of rubber viscoelasticity. Mechanics Research Communications 12:93–99
Miehe C (1988) Zur numerischen Behandlung thermomechanischer Prozesse. Dissertation, Institut für Statik und Dynamik der Luft- und Raumfahrtkonstruktionen Universität Stuttgart
Mooney M (1940) A theory of large elastic deformation. Journal of Applied Physics 11:582–592
Mullins L (1948) Effect of stretching on the properties of rubber. Rubber Chemistry and Technology 21(2):281–300
Naumann C, Ihlemann J (2011) Thermomechanical material behaviour within the concept of representative directions. In: Constitutive Models for Rubber VII, Balkema Leiden, pp 107–112
Payne AR (1962) The dynamic properties of carbon black-loaded natural rubber vulcanizates. part i. Journal of applied polymer science 6(19):57–63
Reese S (2001) Thermomechanische Modellierung gummiartiger Polymerstrukturen. Habilitation, Bericht-Nr. F01/4 des Instituts für Baumechanik und Numerische Mechanik, Universität Hannover
Rivlin RS (1948-1951) Large elastic deformations of isotropic materials part:vii. Philosophical Transactions of the Royal Society of London Series A, Mathematical and Physical Sciences
Rivlin RS (1997) Some applications of elasticity theory to rubber engineering. In: Collected papers of R. S. Rivlin, Springer, pp 9–16
Rivlin RS, Saunders DW (1951) Large elastic deformations of isotropic materials vii. experiments on the deformation of rubber. Philosophical Transactions of the Royal Society of London Series A, Mathematical and Physical Sciences 243(865):251–288
Schlanger HP (1983) A one-dimensional numerical model of heat transfer in the process of tire vulcanization. Rubber Chemistry and Technology 56(2):304–321
Schröder J, Parra Pelaez G (2019) Erfassung, simulation und bewertung der thermomechanischen schädigungsmechanismen von elastomerbauteilen unter dynamischen mechanischen beanspruchungen ii. FKM-Abschlussbericht Heft 334(FKM-Vorhaben Nr.603)
Schwarzl FR (2013) Polymermechanik: Struktur und mechanisches Verhalten von Polymeren. Springer-Verlag
Shutov AV, Landgraf R, Ihlemann J (2013) An explicit solution for implicit time stepping in multiplicative finite strain viscoelasticity. Comp Meth Appl Mech Engrg 265:213–225
Simo JC, Miehe C (1992) Associative coupled thermoplasticity at finite strains: Formulation, numerical analysis and implementation. Computer Methods in Applied Mechanics and Engineering 98(1):41–104
Simo JC, Taylor RL (1982) Penalty function formulations for incompressible nonlinear elastostatics. Computer Methods in Applied Mechanics and Engineering 35:107–118
Stephan P (2002) Vdi wärmeatlas: Berechnungsblätter für den wärmeübergang. Verein Deutscher Ingenieure
Tobolsky AV (1967) Mechanische Eigenschaften und Struktur von Polymeren. Berliner Union
Tobolsky AV, Mark HF, Bondi AA, Deanin RD, DuPre DB, Gent AN, Mark H, Peterlin A, Rebenfeld L, Samulski E, et al (1971) Polymer science and materials. Wiley-Interscience New York
Treloar L (1975) The physics of rubber elasticity. Oxford University Press, USA
Williams ML, Landel RF, Ferry JD (1955) The temperature dependence of relaxation mechanisms in amorphous polymers and other glass-forming liquids. Journal of the American Chemical Society 77(14):3701–3707